IIETA International Information and Engineering Technology Association
Advancing the World of Information and Engineering

Annales de Chimie - Science des Matériaux
Vol. 49, No. 6, December, 2025, pp. 591-599
Journal homepage: http://iieta.org/journals/acsm

Analysis of the Impact of Metal Coatings on the Optical and Tribological Properties of Polymethyl Methacrylate Polymers

Huda M. Turki*, Najim A. Saad, Qassim A. Al-Jarwany

Department of Polymer Engineering and Petrochemical Industries, College of Materials Engineering, University of Babylon, Babylon 51001, Iraq

Corresponding Author Email: mohammedhuda575@gmail.com

https://doi.org/10.18280/acsm.490602

Received: 10 November 2025
Revised: 11 December 2025
Accepted: 19 December 2025
Available online: 31 December 2025

Keywords:
polymethyl methacrylate, silver thin films, DC sputtering, polymer metallization, surface morphology, optical reflectance

ABSTRACT

Polymethyl methacrylate (PMMA) is widely used in optical windows and protective glazing; however, its low reflectance and limited surface durability constrain its deployment in reflective optical assemblies. Here, nanoscale silver (Ag) layers were deposited on PMMA by direct-current sputtering (2–6 min) and analyzed by X-ray diffraction (XRD), the Fourier-transform infrared spectroscopy (FTIR), Atomic force microscopy (AFM), and UV–visible spectroscopy (UV-Vis) to link early-stage film growth to optical performance. XRD verified FCC-Ag formation, while FTIR indicated negligible modification of the PMMA chemical structure. AFM revealed pronounced topographical evolution with sputtering time, with the mean grain diameter and RMS roughness increasing by approximately 456% and 1123%, respectively, at the longest deposition time. UV-Vis measurements showed that reflectance increased from ≤30% for pristine PMMA to >90% after coating (at least a threefold increase), accompanied by an ~82% reduction in visible transmittance at 550 nm. These results demonstrate that sputtering time provides a single, scalable control knob to convert PMMA from a transparent window into a highly reflective metal-polymer hybrid suitable for protective mirrors and other high-end optical components.

1. INTRODUCTION

Polymethyl Methacrylate (PMMA) is a unique thermoplastic polymer, which is defined from the consideration of its chemical structure [1, 2]. The methyl group (CH_3) next to the carbon-carbon backbone restricts rotation and prevents crystallization. This results in an amorphous, transparent, colorless material [1, 3]. PMMA is light-weight [4], economical [5], and does not contain toxic bisphenol-A compounds [6]. It also has good rigidity and ease of handling as well [7]. It has great fracture resistance due to its high Young's modulus (ΔE) and low elongation at break [8, 9]. PMMA is characterized by glass transition temperature around 100-130℃ and can also be synthesized using a number of different polymerization methods, including free-radical, suspension, and emulsion polymerization [2, 3, 6]. While the above-mentioned advantageous properties are appropriate, the PMMA surface is also limited by its own defects that may contribute to the low stability and functionality during long time of usage [10]. Given all those issues to be coped with, surface modification by means of metallic coatings provides a quite interesting approach to solve these problems [11, 12].

Silver (Ag) was selected as the coating material in this study because of the favorable physical and chemical properties Ag possesses [13]. Silver is a good electrical and thermal conductor, highly reflective and bonded to polymer well. It also resists oxidation [14-16]. This makes it suitable for enhancing the optical features as well as the mechanical strength of PMMA. The silver was deposited by direct current sputtering, a physical vapor deposition technique which can be employed to inert substrates like PMMA. This method is excellent since it gives fast coating, good control of film thickness, large area coverage, and high interfacial bonding without damaging the polymer [17].

The silver-coated PMMA is a good candidate for sensing applications due to the Ag layers which can strengthen the optical reflectance and plasmonic resonance. These enhancements allow optical sensors to achieve higher sensitivity and accommodate applicable fields such as chemical and plasmonic detection systems that require well-defined surface interactions.

Most studies on metallized PMMA emphasize relatively thick coatings or longer deposition conditions, while the behavior of nanoscale Ag layers formed under short DC sputtering times remains insufficiently resolved. In particular, prior work often reports optical trends without establishing a quantitative growth-structure-property linkage that connects early-stage surface evolution (grain size, roughness, and thickness) to the resulting reflectance/transmittance response. As a consequence, the influence of short-time Ag sputtering on PMMA remains unclear, limiting the rational selection of deposition conditions for reflective polymer optics.

In this work, we address this gap by systematically depositing Ag on PMMA using DC sputtering for 2, 4, 5, and

6 min (constant process parameters) and correlating structure and chemistry (XRD/FTIR) with surface morphology (AFM) and optical performance (UV-Vis). The novelty of this study is threefold: (1) it provides a controlled, short-time deposition map (2–6 min) that yields nanoscale Ag coatings (≈23–143 nm) on a polymer substrate; (2) it establishes a direct correlation between AFM-derived morphology (grain size/roughness) and optical response; and (3) it demonstrates the transition of PMMA from low reflectance (≈10–30%) to mirror-like reflectance (> 90%) via a scalable sputtering-time "single-knob" control strategy.

2. EXPERIMENTAL PART

2.1 Materials utilized

PMMA sheets were obtained from Goodfellow. They were manually cut into substrates 2 mm thick and 2 × 2 cm each. These substrates were coated by silver. The sputtering target was a locally made silver disc 50 millimeters in diameter and 1.1 millimeters thick.

2.2 Specimen preparation

Synthesis of the coatings was carried out with direct current sputtering. To ensure that all contaminants were removed, PMMA sheets were cleaned in acetone initially. The second step was the deposition of silver coating by the DC sputtering method. The parameters used during sputtering are as follows in Table 1.

Table 1. Sputtering parameters used for the deposition of Ag coating on the PMMA substrate

Gas	Power (W)	Current (mA)	Voltage (V)	Time (min)	Pressure (mbar)
Ar	200	36	1200	2	2-^10*6
	200	36	1200	4	2-^10*6
	200	36	1200	5	2-^10*6
	200	36	1200	6	2-^10*6

2.3 Characterization techniques

2.3.1 XRD

The crystal structure of the silver films was examined via X-ray diffraction (XRD) with Cu Kα radiation (λ = 1.5406 Å). This kind of structural analysis is the foundational first step in evaluating film quality.

2.3.2 FTIR

The Fourier-transform infrared spectroscopy (FTIR) is a spectroscopic technique for the observation of vibrational, rotational, and other low-frequency modes in a polymer and composite materials. Identifying specific absorption bands associated with certain vibrational modes, it gives a molecular fingerprint. FTIR was employed in this work to characterize the pure PMMA prior to silver deposition, immediately following XRD verification.

2.3.3 AFM

Atomic force microscopy (AFM) is a surface characterization tool that has very high resolution. AFM can perform topography measurement, surface roughness, grain size as well as film thickness on a nanometer-scale level. It uses a sharp point scanning the surface while recording height differences in order to produce accurate images.

2.3.4 UV

Ultraviolet-visible (UV-Vis) spectroscopy is the study of the optical properties of materials, usually between 200 and 800 nm. This method quantifies the absorbed or reflected light during its interaction with the sample. It gives information on electronic transitions, surface properties and structural changes. For polymeric substrates and thin-film coatings, UV-Vis analysis can confirm the presence of deposited layers. It also evaluates how coating thickness affects the optical response. When metallic nanoparticles like silver are introduced, UV-Vis spectra can show surface plasmon resonance (SPR) peaks. These peaks indicate the metallic layer and its interaction with the underlying polymer matrix.

The absorption coefficient spectrum (α) was derived from UV-Vis transmittance (T) using a Beer-Lambert-type approximation for each coated film [18]:

$$\alpha(\lambda) = \frac{1}{t}\ln\left(\frac{1}{T(\lambda)}\right) \quad (1)$$

where, T(λ) is the measured transmittance expressed as a fraction and (t) is the Ag film thickness (cm) determined from AFM.

The extinction coefficient was obtained from [19, 20]:

$$k(\lambda) = \frac{\alpha(\lambda)\lambda}{4\pi} \quad (2)$$

where, λ is the wavelength in cm.

3. RESULT AND DISCUSSION

3.1 XRD

XRD measurements were carried out using a Dx2700AB powder multifunction X-ray diffractometer equipped with an SDD detector (Japan), operated using Cu Kα1 with λ = 1.54056 Å (0.154056 nm) at 30 kV/30 mA. XRD analysis of pure silver showed sharp diffraction peaks at 2θ ≈ 38.1˚, 44.3˚, 64.5˚, and 77.5˚. These matched the (111), (200), (220), and (311) planes of face-centered cubic (FCC) silver. The sharp peaks confirm both the crystalline nature and purity of the Ag target used for coating as shown in Figure 1.

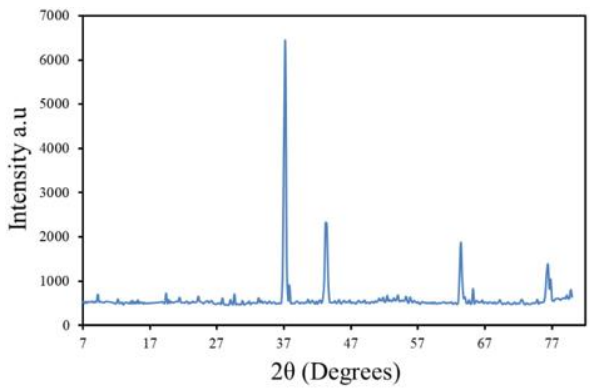

Figure 1. XRD pattern of pure silver (Ag) showing FCC crystal structure with characteristic diffraction peaks (JCPDS card No. 04-0783)

For 2 min (Ag/DC sputtering on PMMA), as shown in Figure 2. The diffractogram exhibits two dominant broad maxima at 2θ ≈ 13.8° and 28.8°, matching the diffuse PMMA features reported at ~13.8° and ~29.7° for amorphous PMMA. The lack of sharp Bragg reflections is consistent with an amorphous polymer matrix where scattering originates mainly from short-range chain packing rather than long-range crystallinity. At this shortest deposition time, Ag is expected to nucleate as discrete islands before forming a continuous film, which can suppress well-defined FCC-Ag reflections in conventional θ-2θ scans. Moreover, diffraction signals from a thin film can be weak relative to the substrate/background in standard geometries, so ultrathin Ag contributions can be masked even if present.

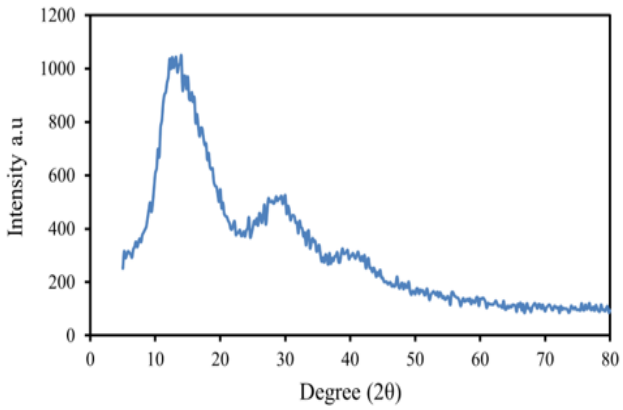

Figure 2. XRD of Ag/PMMA (2 min): broad amorphous maxima at 2θ ≈ 13.8° and 28.8°

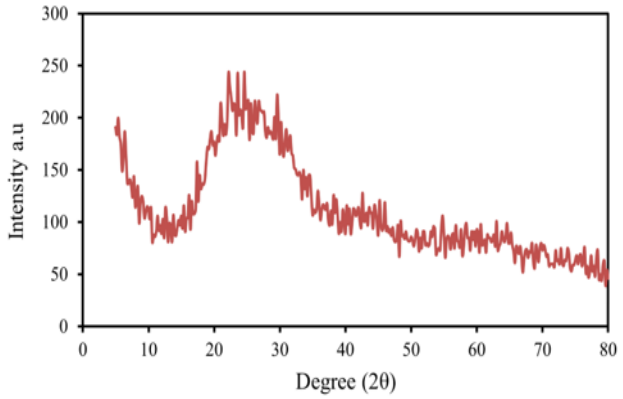

Figure 3. XRD of Ag/PMMA (4 min): single broad halo centered at 2θ ≈ 24.0°

For 4 min (Ag/DC sputtering on PMMA), as shown in Figure 3. The 4 min pattern is dominated by a single broad halo centered at 2θ ≈ 24.0°, indicating predominantly short-range order rather than long-range crystallinity. Compared with 2 min, the PMMA-related maxima are less resolved, which is consistent with increasing Ag coverage producing stronger diffuse scattering during island coalescence and percolation. The nucleation → island growth → coalescence → continuous-film sequence in Volmer-Weber growth is well established, and the coalescence/percolation regime is commonly associated with heterogeneity that degrades diffraction feature definition. Additional loss of clarity is consistent with microstructural peak broadening driven by nanoscale crystallites and lattice strain, which are recognized contributors to reduced peak sharpness/contrast in XRD.

At 5 min, illustrated in Figure 4, broad maxima at 2θ ≈ 13.8° and 28.6° reappear and again coincide with the characteristic diffuse PMMA peaks reported near ~13.8° and ~29.7°. The improved definition relative to 4 min is consistent with Ag films progressing beyond the percolation threshold toward a more continuous layer, reducing the extreme heterogeneity typical of coalescing islands. DC sputtering of Ag on PMMA is reported to produce Ag/PMMA film systems in which film structure evolves with deposition, supporting a transition toward more stable morphology with longer deposition [21].

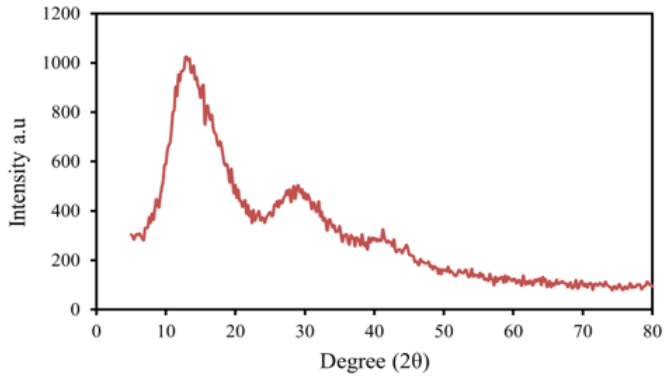

Figure 4. XRD of Ag/PMMA (5 min): diffuse maxima reappear at 2θ ≈ 13.8° and 28.6°

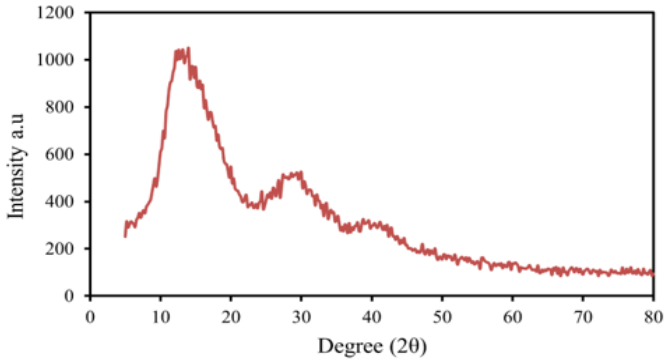

Figure 5. XRD of Ag/PMMA (6 min): stabilized diffuse maxima at 2θ ≈ 13.8° and 28.8°

At 6 min, as shown in Figure 5, the dominant broad maxima remain at 2θ ≈ 13.8° and 28.8°, consistent with the amorphous PMMA diffuse peaks reported at ~13.8° and ~29.7°. Sustaining similar peak positions while the overall pattern stabilizes is consistent with continued Ag overlayer evolution rather than a phase change in the PMMA matrix. Longer sputtering time is a standard driver for increased Ag film thickness in sputtered Ag nanofilms. In standard geometry, thin-film diffraction remains weak compared to the substrate and background, while nanoscale structures and strain broaden any reflections from silver (Ag).

3.2 FTIR

As shown in Figure 6, the FTIR spectrum of pristine PMMA exhibits a strong absorption band at 1722 cm^{-1}, assigned to the ester C=O stretching vibration. Bands at 2994 and 2950 cm^{-1} correspond to aliphatic C-H stretching, while the 1483-1442 cm^{-1} region is associated with CH_3/CH_2 deformation (bending) modes. The band at 1239 cm^{-1} is attributed to ester C-O (C-O-C) stretching, and additional characteristic PMMA fingerprint

vibrations appear at 986, 840, and 749 cm^{-1}. Overall, the spectrum is consistent with the typical functional groups of PMMA, with no extra bands indicative of new chemical functionalities.

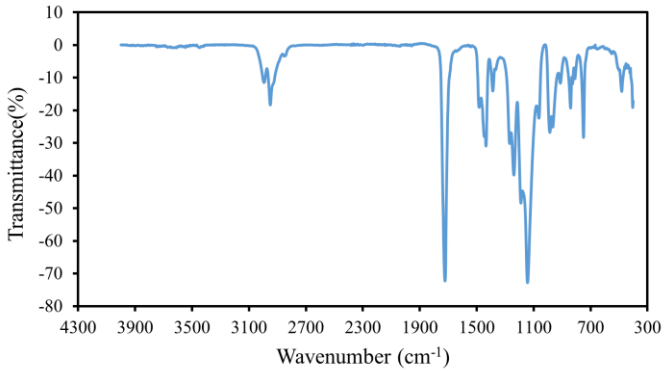

Figure 6. FTIR spectrum of pure PMMA

The 2-min coated sample still shows the PMMA ester carbonyl near ~1733 cm^{-1} and a residual polymer C-O-related band around ~1090 cm^{-1}, indicating that the PMMA functional groups remain present after brief metal deposition. The band near ~2920 cm^{-1} lies within the well-known 2920-2850 cm^{-1} aliphatic C-H stretching envelope typical for polymer chains and commonly used as a backbone marker in FTIR. The feature at ~2359 cm^{-1} is attributable to atmospheric CO_2 (asymmetric stretch fundamental near 2350 cm^{-1}) and typically appears when purge/background compensation is incomplete. The apparent loss of band sharpness relative to pristine PMMA is consistent with early-stage sputtered Ag forming a discontinuous/porous (island-type) layer whose strong scattering and evolving effective optical constants distort the baseline and reduce spectral contrast shown in Figure 7.

At 5 min, the spectrum displays many well-resolved PMMA bands—~2952 and ~2851 cm^{-1} (C-H stretching envelope), ~1725 cm^{-1} (ν(C=O)), ~1449 and ~1389 cm^{-1} (CH_3/CH_2 deformations), and ~1242/1145/1064 cm^{-1} (C-O/CH_3-related modes)—which are all consistent with established PMMA assignments. The clearer emergence of rocking/bending fingerprints at ~990-913 cm^{-1} and ~842-751 cm^{-1} is also consistent with reported PMMA rocking and carbonyl out-of-plane modes in this region. Compared with 2 min, the improved definition is consistent with longer deposition driving Ag from isolated islands toward a percolated/continuous film with higher reflectance and more stable optical response, which increases measurement reproducibility and band contrast. Because Ag incorporation into PMMA is commonly physical (no new covalent-bond bands) rather than chemical, the persistence of the same PMMA functional-group bands with intensity/clarity changes is a typical outcome when Ag is introduced as a separate phase, which is illustrated in Figure 8.

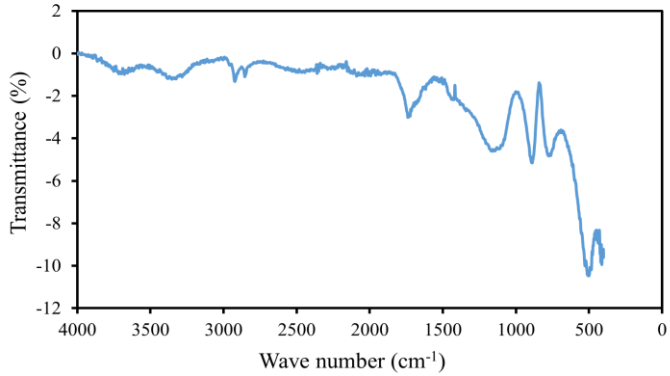

Figure 7. FTIR of Ag/PMMA (2 min): PMMA C=O band ≈ 1733 cm^{-1} retained

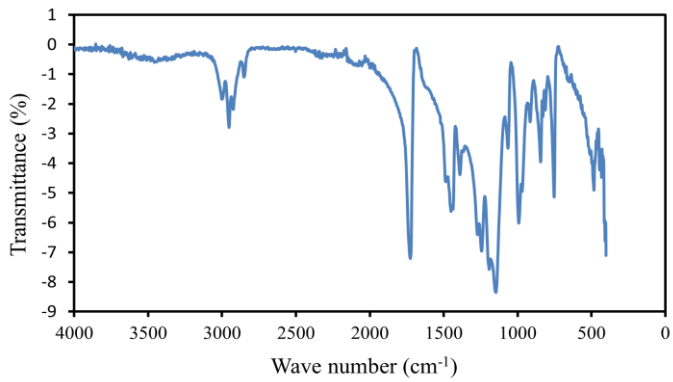

Figure 8. FTIR of Ag/PMMA (5 min): well-resolved PMMA bands with ν(C=O) ≈ 1725 cm^{-1}

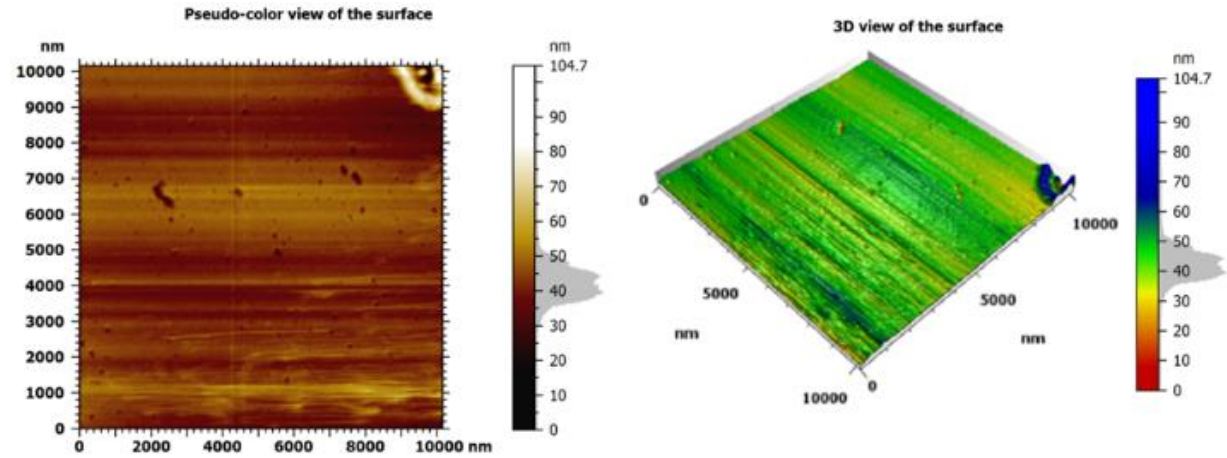

Figure 9. 2D and 3D image of pure PMMA surface

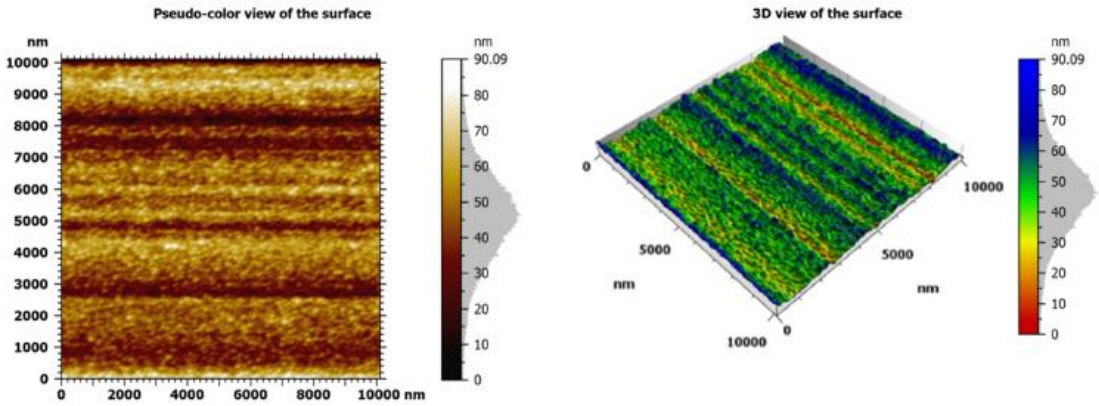

Figure 10. 2D,3D images of Ag deposition after 2min on PMMA substrate

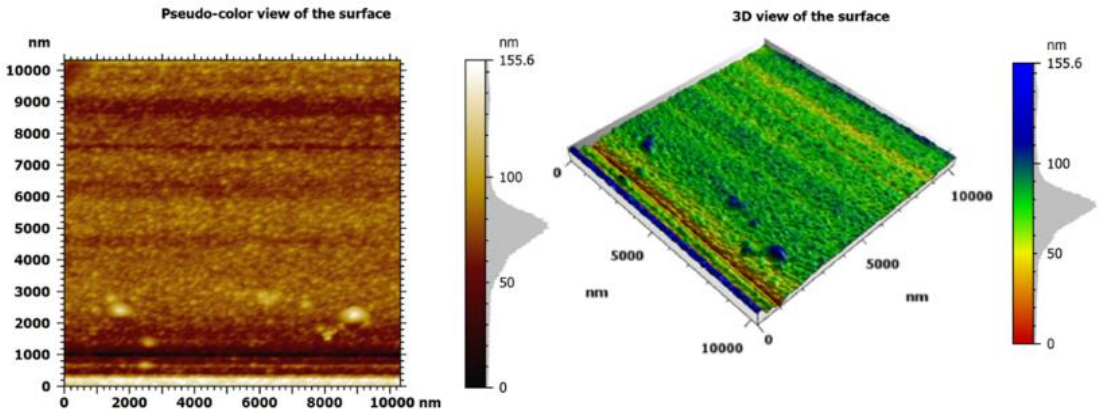

Figure 11. 2D and 3D images after 4min of Ag deposition on PMMA substrate

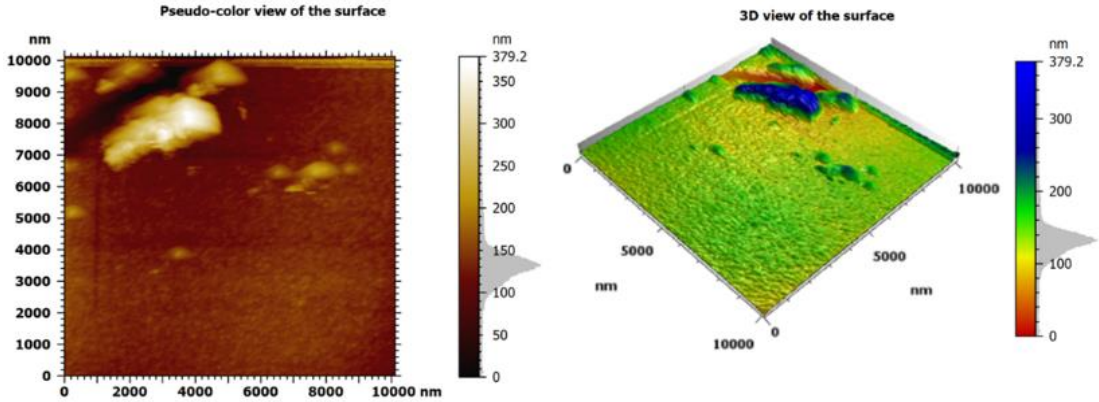

Figure 12. 2D and 3D image after 5 min of Ag deposition on PMMA substrate

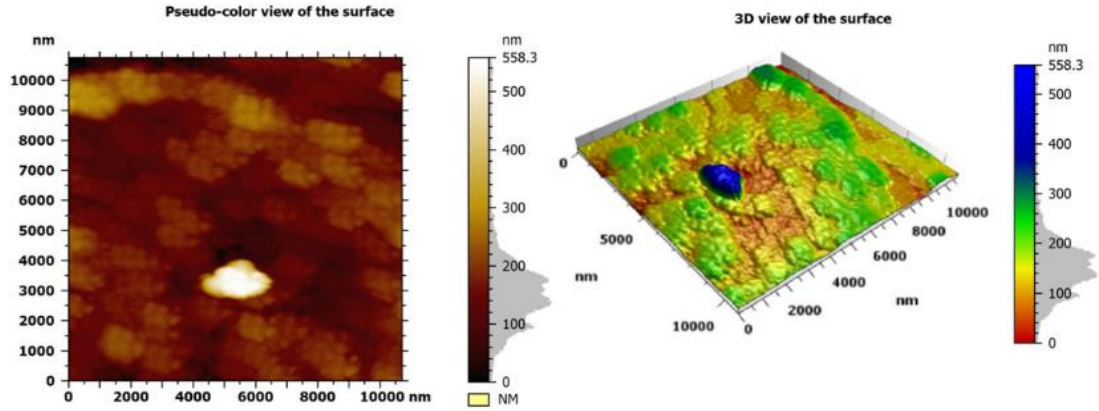

Figure 13. 2Dand 3D image after 6 min of Ag deposition on PMMA substrate

3.3 Atomic force microscopy

As shown in Figures 9-13, AFM 2D and 3D images illustrate the progressive evolution of the surface morphology. The 2D and 3D AFM images showed a gradual increase in surface roughness, grain size, and film thickness with longer silver deposition times. The pure PMMA surface appeared smooth and uniform. In contrast, coated samples exhibited a rougher texture due to silver nanoparticle growth and agglomeration.

Measured grain size increased from a few tens of nanometers in the 2-minute sample to larger, more connected clusters at 6 minutes. Film thickness also increased with sputtering time, confirming continued silver layer formation. Prolonged coating aids particle coalescence and surface coverage, improving the film's metallic character.

The AFM 2D and 3D images of Figures 9–13, along with the quantitative parameters listed in Table 2, clearly indicate a systematic evolution of the PMMA surface when Ag sputtering time is increased. The morphology of this uncoated PMMA substrate in Figure 9 is relatively smooth and has a mean grain diameter of 28.8 nm, along with an under low average rough value of Sa ≈ 3.8nm. After 2 min of Ag deposition Figure 10, discrete metallic clusters are formed on the polymer surface, and the mean grain size increases to 86.7 nm, accompanied by a rise in roughness to Sa ≈ 9.3 nm and Sq ≈ 11.7 nm. Further increasing the sputtering time to 10 and 11 min (Figures 11 and 12) leads to more closely packed features and partial coalescence of the Ag islands, with thickness increasing from 23.5 to 86.4 nm and the roughness almost doubling between 4 and 5 min (SaS_aSa from 11.1 to 22.2 nm). At 6 min (Figure 13), the surface is dominated by larger connected metallic aggregates, the mean grain diameter reaches about 160.4 nm (≈5.6-fold larger than bare PMMA), and the roughness parameters increase by about one order of magnitude (SaS_aSa from 3.8 to 42.8 nm and SqS_qSq from 5.1 to 62.5 nm), indicating the formation of a thicker, more continuous, and topographically complex Ag layer.

Table 2. AFM Surface parameters, film thickness, and mean grain size of PMMA/Ag samples deposited at different times

Samples	Thickness (nm)	Sa (nm)	Sq (nm)	Mean Diameter (nm)
PMMA (Base)	-	3.802	5.109	28.84
2min	23.49	9.259	11.74	86.73
4min	54.83	11.06	16.98	94.72
5min	86.35	22.18	38.9	96.02
6min	142.7	42.83	62.50	160.4

Overall, the evolution observed in Figures 9–13, from isolated Ag clusters at short sputtering times to a thicker and more continuous metallic network at 6 min, provides a clear microstructural explanation for the measured increase in reflectance and the concomitant decrease in transmittance of the PMMA/Ag films. This direct correlation between AFM-derived grain size/roughness and optical response is consistent with previous reports on metal-coated PMMA and related polymer substrates, confirming that the present AFM results are both internally coherent and in line with established behavior for metallic and hybrid polymer coatings.

3.4 UV

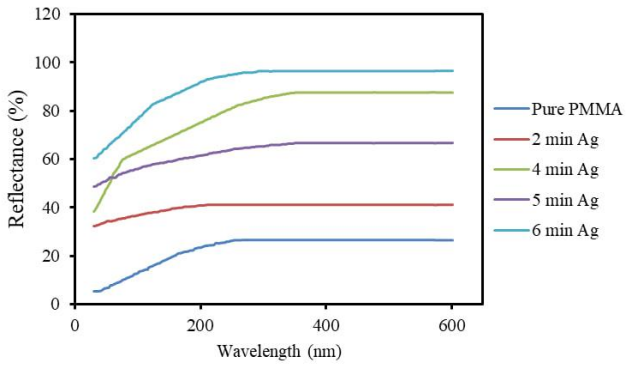

Figure 14. Uv-vis reflectance spectra of silver-coated PMMA

The optical behavior of pure PMMA and Ag-coated PMMA films was investigated using UV-Vis spectroscopy between 300 and 900 nm. Analysis of the reflectance spectra showed that reflection increased with longer silver deposition time. Pure PMMA showed low reflectance (about 10-30%). The 6-minute Ag-coated film showed reflectance above 90% at longer wavelengths. This is due to the formation of a denser metallic layer, which improves light reflection efficiency by the surface plasmon resonance of silver nanoparticles as shown in Figure 14.

The opposite trend is evidenced by the transmittance curves. Pure PMMA achieved the highest transmittance (about 90%). In contrast with the increase in the Ag dosage, the transmittance decreased, with values lower than 20% reached at about 6 min. It makes less dense, but shallower light. The intermediate stages between these semi-transparent and fully reflective films have been described as a function of the coating time: 2 and 4 minutes as shown in Figure 15.

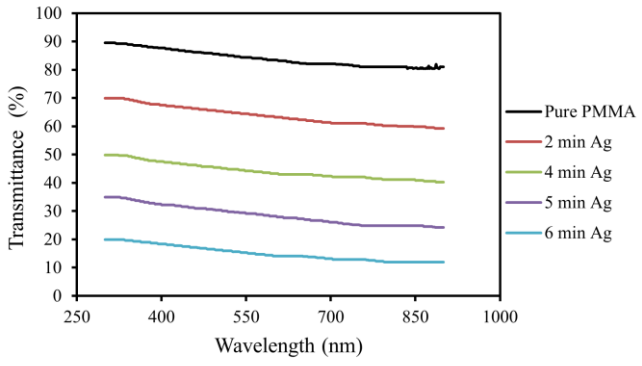

Figure 15. Uv-vis transmittance spectra of silver-coated PMMA

The UV-Vis transmittance spectra (300-900 nm) indicate that pristine PMMA is highly transparent in the visible region, while Ag sputtering causes a systematic reduction in transparency with increasing deposition time. In the 400-700 nm range, the average transmittance decreases from 84.44%

(PMMA) to 64.35% (2 min), 44.51% (4 min), 29.31% (5 min), and 15.52% (6 min), and at 550 nm it decreases from 84.33% to 64.41%, 44.18%, 29.16%, and 15.36%, respectively. This monotonic loss in transmission is consistent with increasing Ag thickness/coverage and the evolution of ultrathin Ag from discontinuous/island-like morphology toward percolated/continuous films, which increases effective optical losses and reflectance. At 550 nm, the calculated effective attenuation coefficient decreases from 1.873×10^5 cm^{-1} (2 min) to 1.490×10^5 cm^{-1} (4 min), 1.427×10^5 cm^{-1} (5 min), and 1.313×10^5 cm^{-1} (6 min), while the overall transmittance continues to drop due to the increasing Ag thickness/coverage. Accordingly, the extinction coefficient at 550 nm decreases from 0.820 to 0.652, 0.625, and 0.575 for 2, 4, 5, and 6 min, respectively, reflecting thickness- and microstructure-dependent optical behavior of the Ag layer. These quantitative values are summarized in Table 3 below.

Table 3. Summary of thickness and quantitative UV-Vis parameters

Sample	Thickness (nm)	Tavg (400-700 nm) %	T(550 nm) %	α(550 nm) (cm^{-1})	k(550 nm)
Pure PMMA	—	84.44	84.33	—	—
2 min Ag	23.49	64.35	64.41	1.873×10^5	0.820
4 min Ag	54.83	44.51	44.18	1.490×10^5	0.652
5 min Ag	86.35	29.31	29.16	1.427×10^5	0.625
6 min Ag	142.7	15.52	15.36	1.313×10^5	0.575

3.5 Adhesion

These approach/retract force-distance curves quantify AFM tip-surface adhesion (via the pull-off force on retraction) and should not be interpreted as a direct measurement of the Ag/PMMA interfacial adhesion strength of the coating system. All force-distance measurements were performed at 25 ± 2°C and 40% relative humidity using a FlexAFM (Nanosurf, Switzerland) instrument, with a probe/tip angle of 10°.

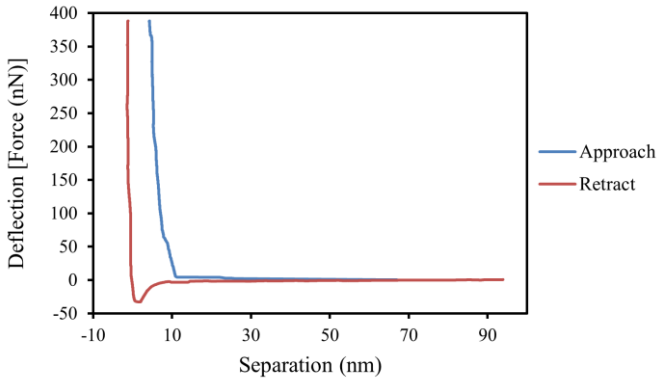

Figure 16. AFM force-distance curve (2 min): Pull-off force −0.03611 µN

For 2 minutes (Ag sputtering time), as shown in Figure 16, the adhesion (pull-off) force extracted from the retraction branch is -0.03611 µN (36.11 nN), which corresponds to the negative minimum just before tip-surface separation and is the standard AFM adhesion metric. The reported snap-in force of -0.003436 µN indicates a measurable attractive instability on approach that is commonly enhanced in ambient air by capillary meniscus formation and humidity-dependent wet adhesion. Because the cantilever spring constant (23.47 N/m) and photodiode sensitivity (101.8 nm/V) are identical across datasets, the force calibration basis is consistent for comparing pull-off between times. At short deposition times, Ag on dielectric/polymeric substrates typically follows Volmer-Weber Island growth before coalescence toward percolation, so the outermost surface can remain laterally heterogeneous. Such heterogeneity can increase variability in local tip-surface interaction because the probe samples a mixed landscape of metallic islands and polymer-exposed regions with different surface energies and wetting behavior. The measured adhesion energy of 0.2330 fJ should be interpreted as an energy-like quantity derived from the retraction curve rather than a direct measure of Ag/PMMA interfacial adhesion strength.

4 minutes (Ag sputtering time), as shown in Figure 17, the adhesion (pull-off) force decreases to -0.03339 µN (33.39 nN), representing a 7.53% reduction relative to 2 minutes under the same calibration constants. This reduction is consistent with continued island coalescence toward a more Ag-dominated top surface as deposition proceeds beyond early Volmer-Weber stages. A practical mechanism for lower pull-off is a reduction in effective real contact area during detachment when nanoscale roughness increases, because roughness can monotonically decrease pull-off in AFM measurements in air. The reported adhesion energy decreases to 0.1848 fJ, which is consistent with a smaller hysteresis-related work term when the detachment interaction is weaker and/or shorter-ranged. The Hertz-fit modulus value (4.201 GPa) should be treated as semi-quantitative because elastic Hertz assumptions are often violated for materials with adhesion and time-dependent deformation in AFM indentation.

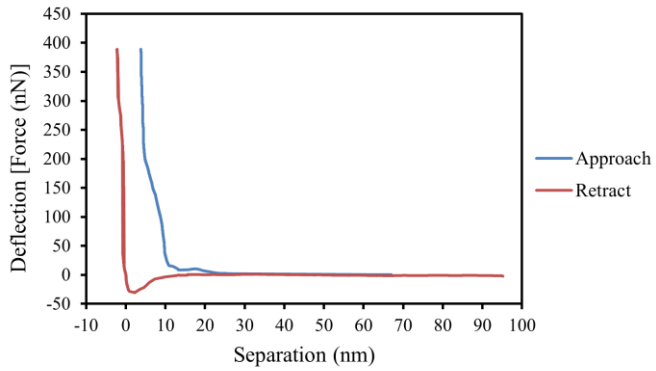

Figure 17. AFM force-distance curve (4 min): Pull-off force -0.03339 µN

5 minutes (Ag sputtering time), as illustrated in Figure 18, the adhesion (pull-off) force further decreases to -0.02672 µN (26.72 nN), corresponding to a 26.00% reduction relative to 2 minutes and a 19.98% reduction relative to 4 minutes. A conservative, single-cause interpretation for the lower pull-off is that further microstructural evolution of the Ag top surface plausibly increases effective nanoscale roughness, which can reduce pull-off by lowering real contact area at separation. The

reported stiffness drops to 0.09516 μN/nm, suggesting a softer apparent contact response in this dataset, which commonly indicates that contact-mechanics outputs can be sensitive to adhesion and viscoelastic effects rather than reflecting a purely elastic solid. The reported Hertz-fit modulus decreases to 1.572 GPa, which should be interpreted cautiously because Hertz-based fits can yield substantially different apparent moduli when time-dependent deformation and adhesion contribute to the force-indentation response. Although pull-off decreases, the adhesion energy increases to 0.2821 fJ, which is feasible because the energy term depends on the integral/hysteresis area and interaction range, not solely on the peak pull-off magnitude. In ambient conditions, time-dependent adsorption on noble-metal surfaces (including Ag) can reduce apparent surface energy and alter wet adhesion, so uncontrolled surface aging and humidity remain plausible contributors even when deposition parameters are identical.

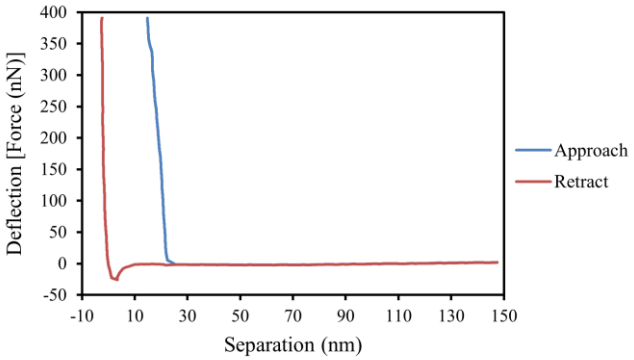

Figure 18. AFM force-distance curve (5 min): Pull-off force −0.02672 μN

4. CONCLUSION

Short-time DC sputtering enables rapid metallization of PMMA with nanoscale Ag films. Increasing deposition time from 2 to 6 min raises Ag thickness from 23.49 to 142.7 nm and promotes a morphological transition from discontinuous islands to a more connected metallic network. This evolution results in a ≥ 200% increase in maximum reflectance (≤ 30% for pristine PMMA to > 90% after coating) and an ~82% decrease in transmittance at 550 nm, while FTIR confirms preservation of PMMA functional groups.

Compared with typical polymer-metallization routes that rely on surface activation or interlayers to improve metal-polymer nucleation/adhesion, the present approach demonstrates mirror-like optical performance within a short deposition window using Ag thicknesses ≤ 142.7 nm. These findings support sputtering time as a practical, scalable control parameter for engineering reflective polymer optics.

ACKNOWLEDGMENT

All praise is due to Allah, whose constant grace and mercy enabled me to accomplish this work. I would like to express my deepest gratitude to my supervisors, Prof. Najim A. Saad and Prof. Qassim A. Al-Jarwany, for their invaluable support, guidance, and constructive advice throughout the course of this study. My sincere thanks are also extended to everyone who assisted me at the College of Materials Engineering.

REFERENCES

[1] Mark, J.E. (2007). Physical Properties of Polymers Handbook. New York: Springer. https://doi.org/10.1007/978-0-387-69002-5

[2] Yousefi, F., Mousavi, S.B., Heris, S.Z., Naghash-Hamed, S. (2023). UV-shielding properties of a cost-effective hybrid PMMA-based thin film coatings using TiO2 and ZnO nanoparticles: A comprehensive evaluation. Scientific Reports, 13(1): 7116. https://doi.org/10.1038/s41598-023-34120-z

[3] Sansul, S., Yousif, E., Zainulabdeen, K. (2023). A review study of the structure, properties and general application of poly (methyl methacrylate). Characterization and Application of Nanomaterials, 6(1): 2537.

[4] Khosroshahi, F.B., Raffan-Montoya, F., Stoliarov, S.I. (2025). Characterization of flammability and species yields for PMMA burning at constant equivalence ratios in a Fire Propagation Apparatus. Fire Safety Journal, 158: 104532. https://doi.org/10.1016/j.firesaf.2025.104532

[5] Godiya, C.B., Marcantoni, E., Dunjić, B., Tomić, M., Nikolić, M.S., Maletaškić, J., Djonlagić, J. (2021). Effect of organoclay modifier structure on the viscoelastic and thermal properties of poly (methyl methacrylate)/organoclay nanocomposites. Polymer Bulletin, 78(6): 2911-2932. https://doi.org/10.1007/s00289-020-03248-7

[6] Yuan, M., Huang, D., Zhao, Y. (2022). Development of synthesis and application of high molecular weight poly(methyl methacrylate). Polymers, 14(13): 2632. https://doi.org/10.3390/polym14132632

[7] Kouicem, M.M., Tomasella, E., Bousquet, A., Batisse, N., Monier, G., Robert-Goumet, C., Dubost, L. (2021). An investigation of adhesion mechanisms between plasma-treated PMMA support and aluminum thin films deposited by PVD. Applied Surface Science, 564: 150322. https://doi.org/10.1016/j.apsusc.2021.150322

[8] An, J., Ding, N., Zhang, Z. (2022). Mechanical and antibacterial properties of polymethyl methacrylate modified with zinc dimethacrylate. The Journal of Prosthetic Dentistry, 128(1): 100-e1. https://doi.org/10.1016/j.prosdent.2022.04.029

[9] Nejatian, T., Nathwani, N., Taylor, L., Sefat, F. (2020). Denture base composites: Effect of surface modified nano- and micro-particulates on mechanical properties of polymethyl methacrylate. Materials, 13(2): 307. https://doi.org/10.3390/ma13020307

[10] Sanjay, S.T., Kannan, S., Li, X. (2025). Simple surface modification of poly (methyl methacrylate) microfluidic microplates for enhanced ultrasensitive multiplexed detection of infectious diseases. Advanced Sensor and Energy Materials, 4(2): 100142. https://doi.org/10.1016/j.asems.2025.100142

[11] Forte, M.A., Silva, R.M., Tavares, C.J., Silva, R.F.E. (2021). Is poly(methyl methacrylate) (PMMA) a suitable substrate for ALD?: A review. Polymers, 13(8): 1346. https://doi.org/10.3390/polym13081346

[12] Melentiev, R., Yudhanto, A., Tao, R., Vuchkov, T., Lubineau, G. (2022). Metallization of polymers and composites: State-of-the-art approaches. Materials & Design, 221: 110958. https://doi.org/10.1016/j.matdes.2022.110958

[13] Valerini, D., Tammaro, L., Vitali, R., Guillot, G., Rinaldi, A. (2021). Sputter-deposited Ag nanoparticles

on electrospun PCL scaffolds: Morphology, wettability and antibacterial activity. Coatings, 11(3): 345. https://doi.org/10.3390/coatings11030345
[14] Daniel, T.O., Nwankwo, U. (2025). Synthesis and characterization of silver/silver oxide thin film via chemical bath deposition. Revista Mexicana de Física, 71(1): 011003-1.
[15] Li, S., Cao, M., Yang, J., Guo, X., Sun, X.F., Wang, T., Qi, Y.S., Li, L.H., Zeng, H.B., Sun, M. (2023). Oxygen plasma-induced conversion of silver complex ink into conductive coatings. Coatings, 13(12): 1977. https://doi.org/10.3390/coatings13121977
[16] Franz, K.J., Metzler-Nolte, N. (2019). Introduction: Metals in medicine. Chemical Reviews, 119(2): 727-729. https://doi.org/10.1021/acs.chemrev.8b00685
[17] Baptista, A., Silva, F.J.G., Porteiro, J., Míguez, J.L., Pinto, G., Fernandes, L. (2018). On the physical vapour deposition (PVD): Evolution of magnetron sputtering processes for industrial applications. Procedia Manufacturing, 17: 746-757. https://doi.org/10.1016/j.promfg.2018.10.125
[18] Saleh, B.E., Teich, M.C. (2019). Fundamentals of Photonics, 2 Volume Set. John Wiley & Sons.
[19] Born, M. (1999). Principles of Optics: Electromagnetic Theory of Propagation, Interference and Diffraction of Light. 7th ed. Cambridge University Press. https://doi.org/10.1017/CBO9781139644181
[20] Fox, M. (2010). Optical Properties of Solids. Oxford University Press, 3.
[21] Mohammed Ali, A.N., Ali, N.A., Hussein, S.I., Hakamy, A., Raffah, B., Alofi, A.S., Abd-Elnaiem, A.M. (2023). Nanoarchitectonics of silver/poly (methyl methacrylate) films: Structure, optical characteristics, antibacterial activity, and wettability. Journal of Inorganic and Organometallic Polymers and Materials, 33(3): 694-706. https://doi.org/10.1007/s10904-022-02525-4

NOMENCLATURE

D	grain (particle) diameter, nm
h	film thickness, nm
I	discharge current during sputtering, mA
P	discharge power applied to the target, W
R	optical reflectance of the film (dimensionless, often reported in %)
Sa	arithmetic mean surface roughness, nm
Sq	root-mean-square surface roughness, nm
t	sputtering (deposition) time, min
T	optical transmittance of the film (dimensionless, often reported in %)
V	discharge voltage, V

Greek Symbols

θ	diffraction angle in XRD, °
λ	wavelength of incident radiation (XRD / UV-Vis), nm

Subscripts

Ag	related to silver coating / Ag layer
PMMA	related to the PMMA substrate